New trends in the hydrogen energy storage potentials of (8, 8) SWCNT and SWBNNT using optical adsorption spectra analysis: a DFT study

Yahaya Saadu Itas[1] · Abdussalam Balarabe Suleiman[2] · Chifu E. Ndikilar[2] · Abdullahi Lawal[3] · Razif Razali[4] ·
Mayeen Uddin Khandaker[5,9] · Mohammed Kolo[6] · Salisu Tata[1] · Abubakr M. Idris[7,8]

Abstract

We have investigated the hydrogen energy storage potentials of (8, 8) single-walled carbon nanotubes (SWCNTs) and (8, 8) single-walled boron nitride nanotubes (SWBNNTs) using density functional theory. Calculations of the electronic properties of the studied systems were performed using the Perdew, Burke and Ernzerhof (PBE) exchange correlation function of the generalized gradient approximation. The optical adsorption response of the pure and hydrogen-adsorbed systems was determined within G_0W_0 approximations with both RPA and BSE. From the obtained results, it was found that both (8, 8) SWBNNT and SWCNT were stable when the hydrogen molecule was 8.72 m away from the adsorption surface. SWBNNT was found to show stronger adsorption from 5 to 15 eV, which is in the UV range. On the other hand, SWCNT adsorbs hydrogen in the 0–5 eV which falls in the UV–Vis range, with higher adsorption recorded from 0 to 2.4 eV, which corresponds to the visible range. Although both systems adsorb hydrogen, (8, 8) SWCNT is reported to be better than (8, 8) SWBNNT due to its ability to adsorb in the visible region of the electromagnetic spectrum. Therefore, SWCNT is regarded as a better candidate for hydrogen energy storage under ambient conditions.

1 Introduction

Today, pollution from burning fossil fuels create an environmental threat to clean ecosystems and domestic water bodies [1]. In addition, by-products of burning fossil fuels pose a major threat to children's health and global environmental instability such as climate change and greenhouse effects [2]. Also, it could run out in the next 50 years due to overuse of fossil fuels. In addition, fossil fuels are non-renewable, their products such as carbon monoxide, ammonia, methane

✉ Yahaya Saadu Itas
yitas@basug.edu.ng

Abdullahi Lawal
labdullahi2@live.utm.my

Mohammed Kolo
mkolo@bosu.edu.ng

Salisu Tata
salisutata20@gmail.com

1   Department of Physics, Bauchi State University Gadau, PMB 65, Gadau, Bauchi, Nigeria

2   Department of Physics, Federal University, Dutse, Nigeria

3   Department of Physics, Federal College of Education, Zaria, Nigeria

4   Department of Physics Faculty of Science, Universiti Teknologi, Johor Bahru, Malaysia

5   Present Address: Centre for Applied Physics and Radiation Technologies, School of Engineering and Technology, Sunway University, 47500 Bandar Sunway, Selangor, Malaysia

6   Department of Physics, Borno State University, Maiduguri, Nigeria

7   Department of Chemistry, College of Science, King Khalid University, 62529 Abha, Saudi Arabia

8   Research Center for Advanced Materials Science (RCAMS), King Khalid University, 62529 Abha, Saudi Arabia

9   Faculty of Graduate Studies, Daffodil International University, Daffodil Smart City, Birulia, 1216 Savar, Dhaka, Bangladesh

and sulfides pollute the environment and lead to an ongoing increase in global warming and climate change. The report of the United Nations Intergovernmental Panel on Climate Change, published earlier this year, warned that if we are to limit warming to 1.5 °C, greenhouse gas emissions must fall by 2025 and fall by 43% by 2030 from current levels [3]. To meet this challenge, various researchers are recommending hydrogen as a better alternative to fossil fuels due to its cleanliness, renewability and sustainability, as well as its low impact on the ecosystem. At up to 142 MJ kg^{-1} [4], it is the most abundant element in the Universe, outperforming its fossil fuel counterpart by a factor of three. In addition, the product of hydrogen combustion is water, which is why it does not pollute the ecosystem when burned. Hydrogen can also be used as a fuel for piston engines, gas turbines or hydrogen fuel cells, with the latter offering the best efficiency. Therefore, hydrogen energy research is becoming a topic of greatest interest as it has the potential to replace fossil fuels in many areas of combustion technologies [5].

Although robust experimental results show that hydrogen is the best material for the next-generation energy source, it needs to be stored under appropriate conditions. The main concern in the growth of hydrogen energy technology is safe, efficient and reliable storage facilities [6]. Compressed hydrogen tanks require very high pressures, while liquefied hydrogen requires expensive cryogenic processes. However, these facilities are generally not secure in terms of the usability of energy for the average person. According to the US Department of Energy, the gravimetric target for hydrogen storage for an onboard system is 5.5% by weight by 2020. Consequently, the reversible hydrogen storage capacity of a solid-state material for use in an onboard system must be significantly higher than 5.5% by weight considering the mass of other components. To meet this challenge, various types of researches have been conducted on lightweight solid-state materials, especially lightweight and low-cost carbon nanomaterials, graphite-derived polymorphs and nanostructures including nanotubes [7]. In addition, the decoration of nanomaterials with cheap metals led to significant results in improving hydrogen adsorption efficiency.

Although, notable success has been achieved in providing permanent solutions to hydrogen storage problems. There were too many conflicting results that need improvement as most of these materials failed to meet the requirements for applicable hydrogen storage. For example, carbon nanotubes have been reported to provide a physisorption surface for hydrogen adsorption [8]. However, the literature failed to describe the anisotropic effects and tube orientations in terms of the H-C bond energies. Moreover, a comparison of the H adsorption efficiency of CNTs with similar nanotubes such as boron nitride nanotubes has also not been reported. Also, optoelectronic effects on the H-adsorbed systems such

as optical refraction, transmission and conductivity have not been reported.

In this work, we studied the adsorption of hydrogen by single-walled carbon nanotubes (SWCNT) and single-walled boron nitride nanotubes (SWBNNT) using a new method called optical spectral analysis. SWCNT and SWBNNT were chosen for this work because of the large volume-to-surface area ratio and lightweight properties that are among the properties of materials that absorb hydrogen. In addition, SWBNNT's characteristic porous nature and lighter weight make them interesting candidates for practical hydrogen storage. The absorption efficiencies of the studied SWCNT and SWBNNT structures are compared, and the effects of the dielectric response on the studied systems are also discussed. In addition, the results obtained are checked for correlation with the experimental data.

2 Research methods

In this work, we investigated hydrogen adsorption potentials of (8, 8) armchair SWCNT and (8, 8) armchair SWBNNT using an optical absorption spectra approach. The investigation of all optimized systems was based on the popular density functional theory. Electronic interactions and determination of the band gap of SWCNT and SWBNNT were performed using the generalized gradient approximation method in terms of the Perdew, Burke and Ernzerhof (PBE) [9] exchange correlation functional and norm conserving pseudo potentials. To ensure accurate results, the quasi-particle energy correction was performed via the G_0W_0 approximation implemented in the Yambo code using many-body perturbation theory. We use the MBPT to link N atom and N and N ± 1-particle systems using the central time-ordered Green function [10], given by,

$$G\left(r'\ t', r'\ t'\right) \tag{1}$$

To make balance between computational cost and accuracy, kinetic energy convergence (see Fig. 10) for both nanotubes was performed in steps of 20 Ry, 30 Ry, 40 Ry 60, Ry 80 Ry and 70 Ry while convergence of k-points sampling was performed in steps of $1 \times 1x20$, $1 \times 1x26 \times 1x1 \times 30$ and $1 \times 1x34$. Studies of the optical absorption spectrum were done using the optical response to the incident photon energy in terms of the imaginary dielectric with RPA and BSE. The optical absorption spectra are computed by solving Bethe–Salpeter equation (BSE) within G_0W_0 approximation. BSE approach was chosen in this work because it gives accurate descriptions of the electron–hole interactions and report the exact bound state of the excitonic systems. GW convergence was achieved using plasmon-pole

approximation for the dielectric function and then Newton solver to the quasi-particle correction. Additionally, convergence was done only between the energy differences of the bottom of the conduction band top of the valence band. To achieve balance between computational cost and accuracy, exchange self-energy cutoff and number of bands in the calculation of the dielectric function were all converged.

3 Results and discussion

3.1 Structural properties

In this work, the structural properties of the optimized systems of (8, 8) SWCNT and SWBNNT structures were determined such that the system absorbs hydrogen molecules in a specific three-dimensional space. Figure 1 presents the optimized structures of SWCNT and SWBNNT systems before and after hydrogen interactions, while Table 1 shows
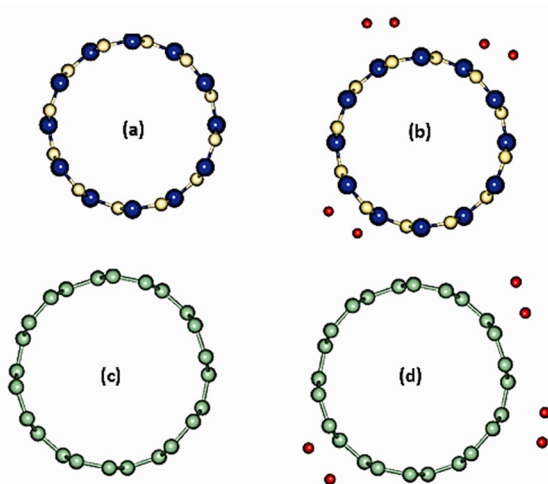

Fig. 1 Optimized structure of **a** pristine SWBNNT, **b** hydrogen-adsorbed SWBNNT, **c** pristine SWCNT and **d** hydrogen-adsorbed SWCNT; the blue calls denote nitrogen atoms, gray ball denotes boron atoms and red balls represent hydrogen atoms while green balls denote carbon atoms

the convergence parameters of the pristine and the hydrogen-absorbing SWCNT and SWBNNT systems with respect to the hydrogen distance. To clearly understand the independent hydrogen adsorption efficiencies of each nanotube, the distance of a hydrogen molecule from the adsorption surfaces (SWCNT and SWBNNT) was uniformly varied to 8.21, 8.72 and 9.31, respectively. Results revealed that the diameter of SWBNNT is larger than that of SWCNT because the bond length of SWBNNT is 0.31 longer than that of SWCNT. In the case of H_2_adsorbed SWCNT, the total adsorption energy was not converged for hydrogen adsorbed 8.21 Å away by SWCNT. However, perfect adsorption occurred as the hydrogen molecule was moved further away from SWCNT to 8.72 Å resulting in a total energy convergence of −537.06 eV. There was also a partial convergence at 9.31 Å. Based on this, we can report that hydrogen was perfectly adsorbed by the (8, 8) SWCNT when they are 8.72 Å away.

In the case of H_2_adsorbed SWBNNT, hydrogen molecule was well adsorbed between 8.21 Å and 8.72 Å. Claim to this corresponds to the negligible change in the total energy of adsorption for the hydrogen situated at 8.21 Å and 8.72 Å, respectively. Based on the results of Table 1, the chosen distance of hydrogen from (8, 8) SWCNT and SWBNNT surfaces for perfect adsorption is 8.72 Å.

3.2 Effects of hydrogen adsorption on the electronic properties of SWBNNT

To get a good understanding of the optical response of the (8, 8) SWBNNT due to hydrogen adsorption, the electronic properties of the SWBNNT structure were calculated using both the KS and G_0W_0 approximations. The band structures were determined along the high symmetry point axis of the irreducible Brillouin zone in which the Fermi level was set at 0 eV. The electronic structure of pristine SWBNNT and H_2-adsorbed SWBNNT is shown in Fig. 2a and 2b. Regarding GGA, the calculated band gap of the original SWBNNT was found to be 4.9 eV. Although this value agrees well with the literature, the problem of a band gap under estimation by GGA has been reported frequently [11]. To correct this,

Table 1 Convergence parameters

Material	Chirality	Diameter (Å)	Hydrogen distance (Å)	Absorption energy (eV)	Remark
H_2_adsorbed SWCNT	(8, 8)	14.32	8.21 Å	-534.42	Energy not converged
	(8, 8)	14.32	8.72 Å	-537.06	Energy converged
	(8, 8)	14.32	9.31 Å	-537.42	Energy partially converged
H_2_adsorbed SWBNNT	(8, 8)	16.64	8.21 Å	-631.93	Energy converged
	(8, 8)	14.64	8.72 Å	-631.93	Energy converged
	(8, 8)	14.64	9.31 Å	-631.92	Energy converged

Fig. 2 Electronic bands of **a** pristine SWBNNT, demonstrating wider direct bands and relatively curved conduction bands and **b** H_2_adsorbed SWBNNT, demonstrating closure of bands by hydrogen molecules and relatively stretched conduction bands
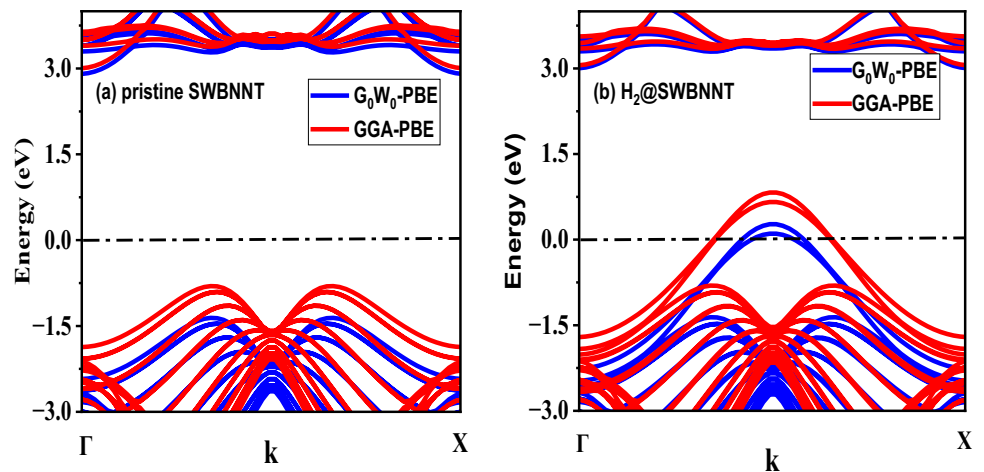
we re-ran the calculation using the one-shot GW approximation, which resulted in a significant blue shift of 5.2 eV, which also corresponds to the true band gap of our studied SWBNNT. Furthermore, the bands formed were direct bands, since the maxima of the equilibrium band and the minima of the conduction band were found to have the same momentum [12]. Therefore, this material generates light during electron–hole recombination, favoring it as a better candidate for hydrogen adsorption under ambient conditions. Regarding the hydrogen-adsorbed SWBNNT (H_2_adsorbed SWBNNT), it was found that hydrogen adsorption through the outer walls of the SWBNNT resulted in a tube reconstruction that closes the band gap and reduces band bending effects. In this case, the band gap changes after hydrogen molecules are adsorbed on the SWBNNT surface, which is in good agreement with the obtained theoretical data. Therefore, our investigation revealed that the carrier mobility of the SWBNNT increases when it engages in physical interactions with hydrogen. Furthermore, the qualitative features obtained from the GGA and GW calculations are identical [13], apart from a rigid shift in the conduction bands (since the valence bands are fixed such that the valence band maximum is 0).

In general, topological behaviors of interacting systems with regard to gas adsorption, in particular their band structure, have a large impact on the density-of-state properties. Furthermore, it has been reported that the density of states outside the band edge can deviate from the expected energy dependence [1]. In order to determine the number of electronic occupations and orbital contributions by pure and hydrogen-adsorbed systems, we measured the total density of states (TDOS) and partial density of states (PDOS). The results of calculations are shown in Fig. 3. Regarding the TDOS for pristine and hydrogen-adsorbed SWBNNT shown in Fig. 3a and b, three distinct peaks are separated by energy gaps in the valence band, while one peak was observed in the conduction band. Empty bands at SWBNNT's Fermi

level justified its semiconducting nature, while the presence bands at Fermi level of H_2_adsorbed SWBNNT proved its metallic properties. Furthermore, more states were observed in pristine SWBNNT because energy occupation increases with band gap, which correlates well with the obtained literature results. Figure 2c shows the PDOS of the pristine and the H_2-adsorbed SWBNNT. An energetically lower valence band is seen in the range -2.2 eV–10.0 eV, mainly due to contributions from the p orbitals of N and also the s orbital of B. Smaller contributions were also observed for the s orbital of nitrogen. The region between -2.2 eV above the Fermi level up to 1.3 eV is mainly the region of hydrogen confinement, as such dominated by s_orbitals of hydrogen. Therefore, the properties of the H_2-adsorbed SWBNNT around the Fermi level are due to s_orbials of hydrogen. The minimum conduction bands originate mainly from the p_ orbital of the B atom, while the maxima of the valence band originate from the p_orbital of the N atom. Based on these results, we can show that SWBNNT provided an adsorption surface area for hydrogen molecules above and below the vicinity of the Fermi level, and this agrees with the results obtained previously, as shown in Table 2.

3.3 Optical properties of pristine and H_2_adsorbed SWBNNT (optical spectra analysis)

To get the right insight into the behavior of the (8, 8) SWBNNT as a result of its interactions with hydrogen molecules, we first calculated its optical properties in pure (pristine) form and then after hydrogen adsorption. The results are presented in Fig. 4a and b. Through investigations from the literature, it was determined that the analysis on the properties of H_2_adsorbed SWBNNT was not performed using optical adsorption spectra analysis. In the present work, we are only interested in the photon absorption by the investigated nanotubes; hence, only imaginary parts of the dielectric function were considered. Furthermore, the
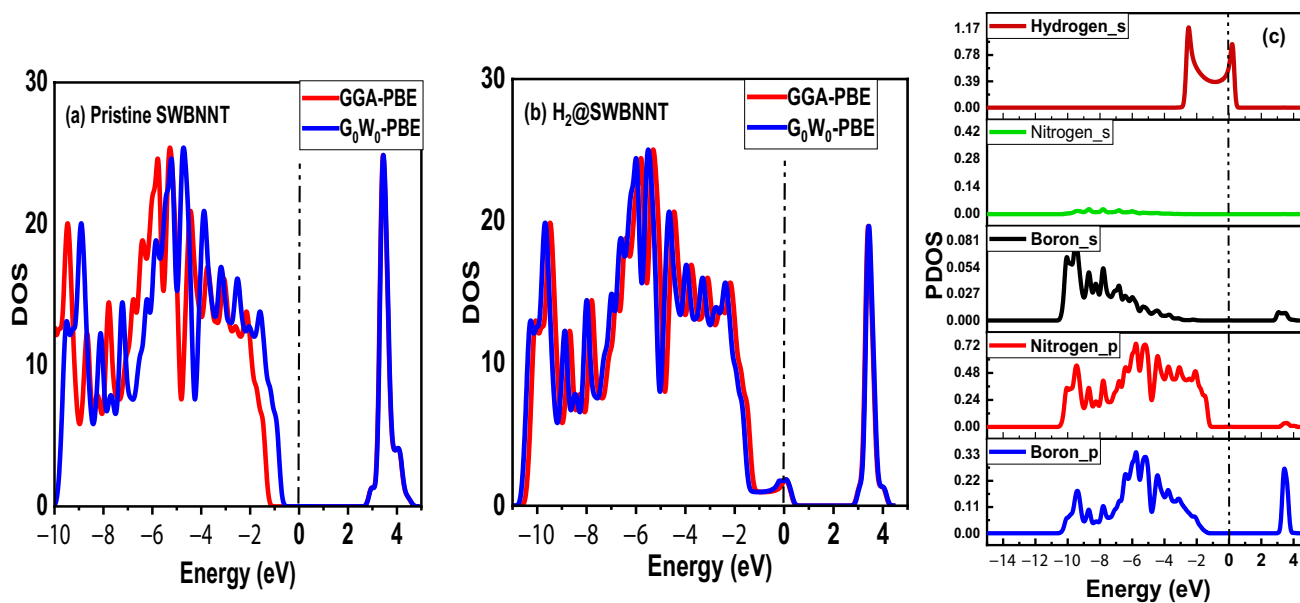
Fig. 3 **a** DOS for pristine SWBNNT with empty states near Fermi level, **b** DOS for H_2_adsorbed SWBNNT, showing occupations at Fermi level and **c** PDOS for H_2_adsorbed SWBNNT showing various orbitals contributions

Table 2 The experimental and calculated band gap for pristine SWBNNT

Method	Band gap (eV)	Nature of band gap
LDA	4.76 [14]	Direct
GGA-PBE	4.8 eV [15]	Direct
G_0W_0	5.2 (This work)	Direct
GGA-PBE	4.8 (This work)	Direct
Experimental	4.92	Indirect

optical band gaps were calculated using both RPA and BSE approaches, considering parallel and perpendicular directions of the considered nanotubes. The GDamping in the Green's function determination was set to 0.1 eV, imaginary dielectric function calculations were performed by extending the Green's function using 25 bands. With respect to SWBNNT, the first critical step was reached at 5.2 eV, which corresponds to the obtained G_0W_0 band gap [16], as shown in Fig. 3a, denoted as the edge of the absorption spectrum.

Fig. 4 Imaginary dielectric constants for pristine SWBNNT under **a** RPA and **b** BSE. As reported, all the spectra showed more intensities in parallel than perpendicular to the nanotubes' axes
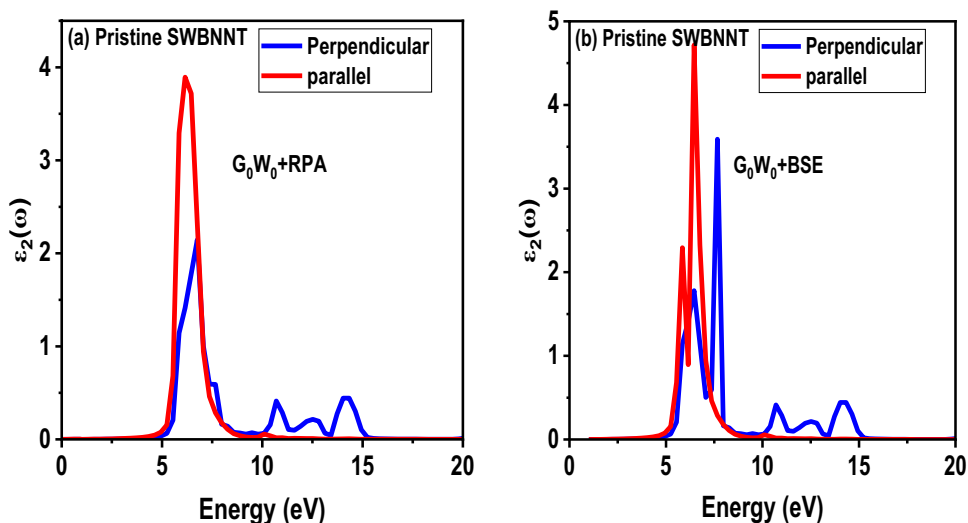
The SWBNNT has been observed to absorb photons above 5 eV, which is in the UV range. Since photon absorption in the UV range accounts for only 3% of the absorbed solar energy, SWBNNT is expected to absorb less heat and is, therefore, best suited for gas adsorption under ambient conditions. In the BSE approach, more adsorption peaks including bound states are shown in Fig. 4b due to the inclusion of the electron–hole interaction. Furthermore, due to the high aspect ratio (length to diameter) and larger surface area of the nanotubes, all of the nanotubes interacted with photons in a parallel rather than a perpendicular direction. Another factor that also contributed to the variation in the optical absorption of the nanotube is its anisotropy.

Results of the interactions of (8, 8) SWBNNT with hydrogen molecules are shown in Fig. 5a and 5b. Figure 5a shows the hydrogen adsorption spectra under RPA without considering the e–h interactions. It can be seen that the (8, 8) SWBNNT interacts with hydrogen in the UV–Vis region.

To support this statement, high-energy adsorption peaks can be seen in both parallel and perpendicular directions to the nanotube in the range of 0.25 eV. By including e–h interactions, more peaks appeared in the parallel direction between 0 eV and 2.8 eV, which corresponds to the region of energy adsorption in the visible spectrum (Fig. 5b). It was also observed that there is no perpendicular adsorption in the visible range. Furthermore, inclusion of the e–h interactions showed that more hydrogen molecules were adsorbed parallel than perpendicular to the axis of the nanotubes. Based on this, we can report that the high surface area and anisotropy of the SWBNNT were preserved after hydrogen adsorption.

3.4 Effects of hydrogen adsorption on the electronic properties of SWCNT

According to the literature, the process of gas adsorption on the surface of metallic material is called occlusion, while the

Fig. 5 Hydrogen adsorption spectra for pristine SWBNNT under **a** RPA and **b** BSE. More occluded hydrogen peaks appear due to electron–hole interactions
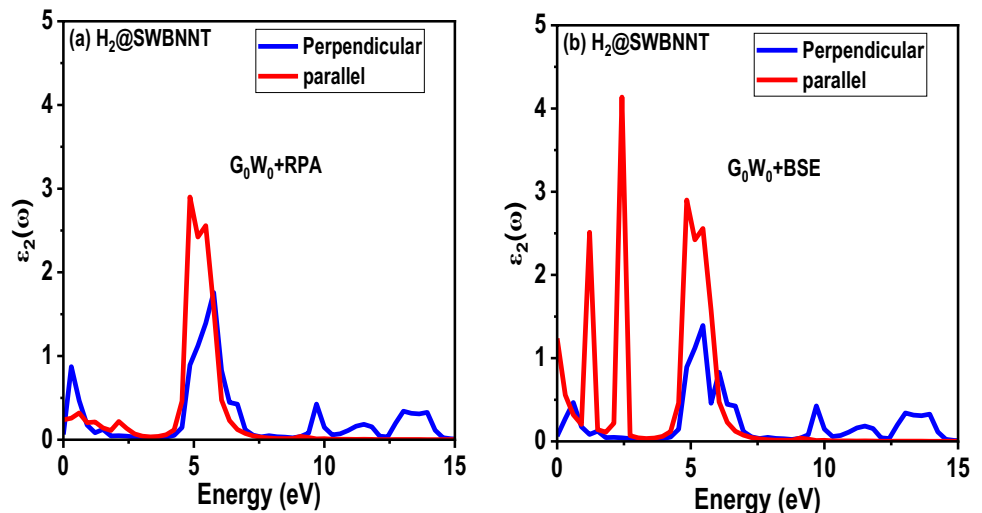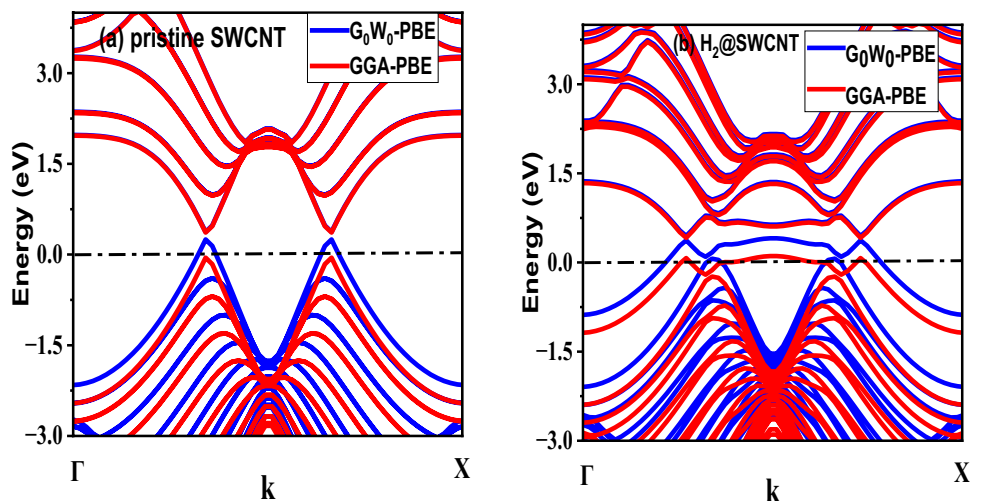

Fig. 6 Electronic band structures of **a** pristine SWCNT and **b** H$_2$_adsorbed SWCNT. Both systems demonstrated metallic behaviors

adsorbed hydrogen is called occluded hydrogen. Furthermore, hydrogen adsorption by non-band gap materials is a result of van der Waals forces between the occluded hydrogen (adsorbate) and the adsorbent. As shown in Fig. 6a, our studied armchair SWCNT showed good metallic [17] properties using the G_0W_0 approximation by showing a zero band gap. Upon adsorption of hydrogen, Fig. 6b shows a change in the occupation of the Fermi level by additional hydrogen molecules, showing that occlusion between hydrogen and SWCNT took place. Band contours formed across the Fermi level were as a result of hydrogen molecules which occupy positions on the surface of the nanotubes due to adsorption. Due to the larger surface area of the nanotube, the heat of adsorption of hydrogen generally decreases. Therefore, the surface of the SWCNT becomes colder during occlusion, favoring it as a better candidate for hydrogen storage than the previously reported SWBNNT. Therefore, the occluded hydrogen molecules stick to the SWCNT surface like condensation of water molecules sticking to a drinking glass. The hydrogen adsorbed by metallic SWCNT can be used in various processes such as activated carbon, catalysts and chilled water for air conditioning. It can also be used for various physical, chemical and biological systems in industry. Moreover, the observed similarities between bands of the pristine SWCNT and the hydrogen-adsorbed SWCNT demonstrated the invariance of the structural properties of the SWCNT due to hydrogen adsorption.

We further investigated the factors influencing the adsorption energy by calculating the electronic density of states (DOS) of the interacting nanotubes. It has also been reported that conformational changes caused by adsorption can dramatically affect a molecule's properties [18]. The DOS plots in Figs. 7a and 6b showed more occupied states in the valence band than in the conduction band. As shown in

Fig. 7b, the intensity of the occupied states decreased upon adsorption of hydrogen molecules, confirming that hydrogen physisorption controls conformation and DOS [18]. In addition, the (8, 8) SWCNT material retains its metallic properties after hydrogen adsorption. Therefore, the trapped hydrogen has no influence on the field emission current of the SWCNT. Compared to pristine SWCNT, the intensity of the DOS of hydrogen-adsorbed SWCNT dropped well below 20 states per energy level. This large shift was due to van der Walls forces, despite the apparent lack of chemical interactions. Therefore, our results indicated that Van der Waals played an important role in determining the key adsorption properties of the SWCNT. The calculated and experimental band gap values for bare (8, 8) SWCNT are presented in Table 3. Results from the table revealed very good agreement with the obtained properties of armchair SWCNTs reported.

The energy of absorptions of both pristine and hydrogen-adsorbed SWCNT was calculated in terms of the imaginary dielectric response. The optical absorption spectrum is defined by the imaginary part of the dielectric function, which can be calculated as follows:

Table 3 The experimental and calculated band gap for pristine SWCNT

Method	Band gap (eV)	Nature of band gap
LDA	0.35	Direct [19]
GGA-PBE	0.41 eV [20]	Direct
G_0W_0	0.00 (This work)	Direct [21]
GGA-PBE	0.40 (This work)	Direct
Experimental	0.01 [22]	Direct

Fig. 7 Electronic DOS of **a** pristine SWCNT and **b** H_2_adsorbed SWCNT. Both systems showed occupied states at Fermi level
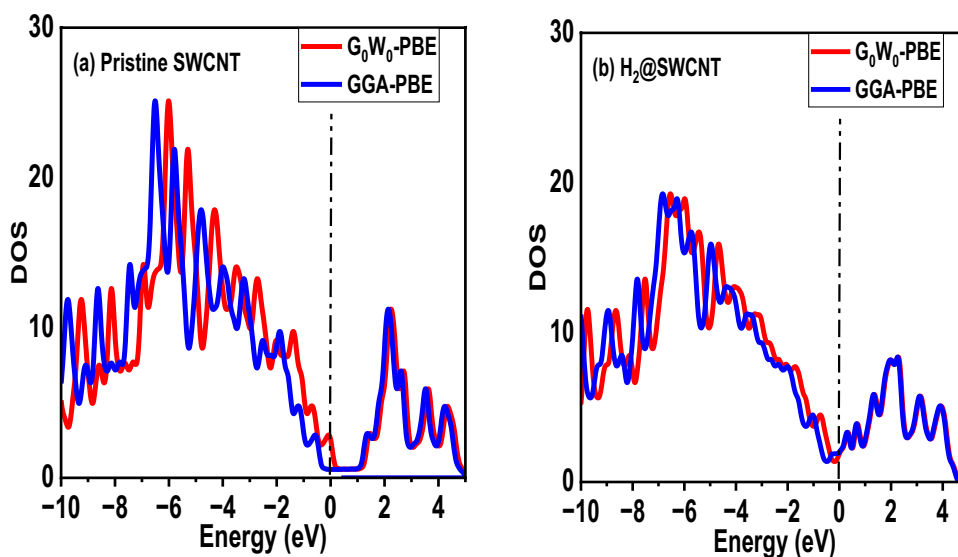
$$\varepsilon_2^{G0W0+BSE}(\omega) = \frac{16\pi e^2}{\omega^2} \sum_S \left| \vec{\lambda}.O|\vec{v}|S \right|^2 \delta(\omega - \Omega^s) \qquad (2)$$

where ε_2 denotes the imaginary dielectric constant which takes care of the amount of hydrogen energy adsorbed, and $G0W0 + BSE$ are quantities which take care of the quasiparticle properties in terms of the electron–hole interactions. The imaginary part of the dielectric function is the result of the summation of the valence to conduction band transitions under a specified k-point of the corresponding BZ. The absorption spectra obtained for the original SWCNT under RPA and BSE are shown in Fig. 8a and b. As shown in Fig. 8b and a, clear optical absorption edge can be seen at 0.3 eV and 0.4 eV in perpendicular and parallel, respectively. Compared to the SWBNNT (previously shown in Fig. 3), the armchair SWCNT absorbs more electromagnetic energy than the SWBNNT. For example, the imaginary dielectric constant for SWBNNT under BSE parallel

was 4.8 (Fig. 4b), while the imaginary dielectric constant for SWCNT was 10 (Fig. 8b). Furthermore, energies in a much lower range (0–5 eV) are absorbed by SWCNT than by SWBNNT (5–8 eV), and this agrees well with the reported experimental data. The obtained spectra for armchair SWCNT after adsorption of hydrogen molecules are shown in Fig. 8a and b.

Figure 9a shows the hydrogen adsorption spectra of (8, 8) SWCNT. As observed, hydrogen molecules were adsorbed in the 0 eV–5 eV range, which corresponds to the UV–Vis range [23]. The highest adsorption was recorded at 2.3 eV, which corresponds to the visible range. In addition, there was a higher adsorption in parallel than perpendicular to the axis of the nanotubes. Claim for this statement was based on the drop in the intensity of the imaginary dielectric value from 22 in the parallel to 7.3 in the perpendicular. Higher parallel adsorption was due to the high aspect ratio characteristic of the nanotube, while lower adsorption in

Fig. 8 Imaginary dielectric constants for pristine SWCNT under **a** RPA and **b** BSE. The spectra showed that SWCNT adsorbs more hydrogen in the visible range
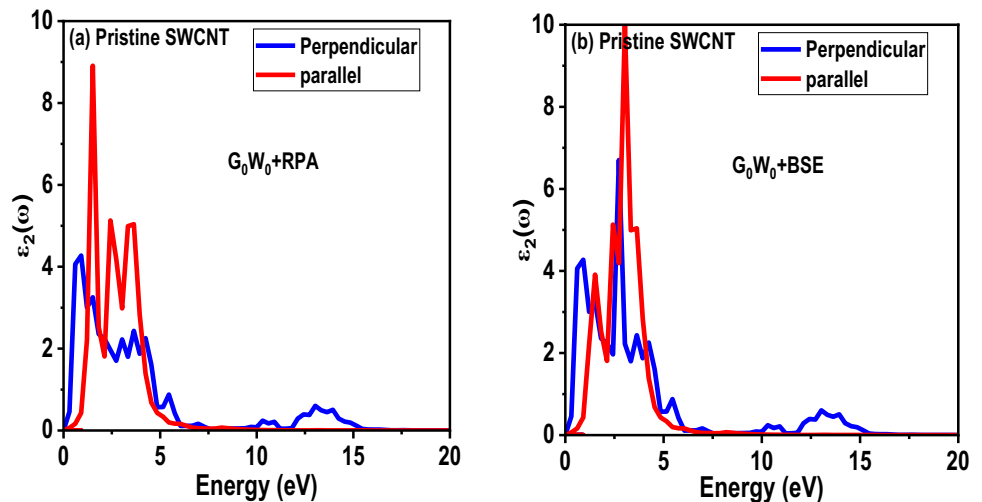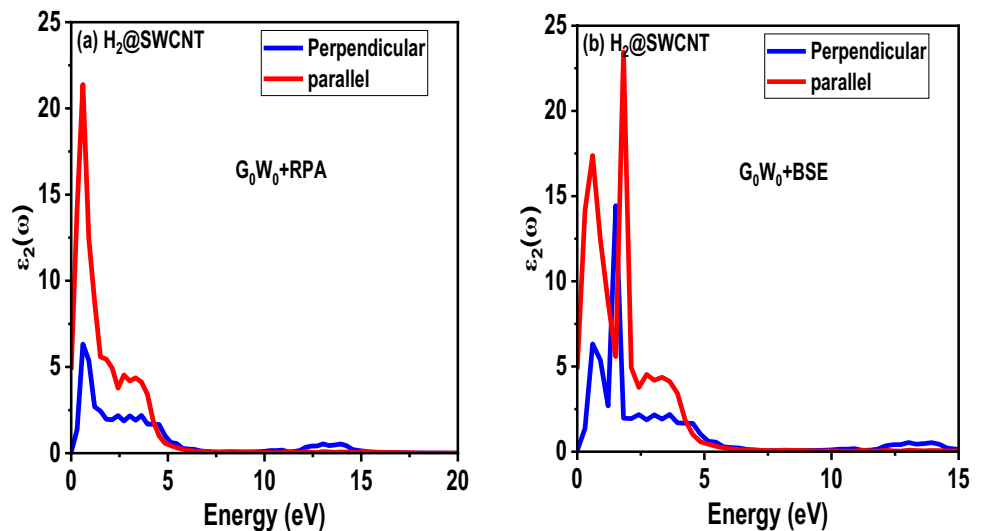

Fig. 9 Hydrogen adsorption spectra for pristine SWCNT under **a** RPA and **b** BSE

the perpendicular direction was due to energy loss along the perpendicular direction caused by a lower diameter-to-length ratio [24]. The effects of including e–h interactions are shown in Fig. 9b. More adsorption peaks appear at 0 eV–2.5 eV in both parallel and perpendicular, which is the optical band gap value for materials used as photocatalysts. Therefore, it can be reported that (8, 8) SWCNT adsorbs hydrogen molecules in a manner similar to a photocatalyst. Another interesting new feature observed in hydrogen-adsorbed (8, 8) SWCNTs is the fact that its geometric and structural properties were retained after adsorption. Several adsorption peaks can be seen due to interactions within the bands of electrons and holes of hydrogen and carbon atoms. Another advantage of hydrogen adsorption by chair SWC-NTs over SWBNNTs is their ability to be efficient under ambient conditions, hence providing a cheap facility for hydrogen energy storage. The energy storage potentials of both SWCNT and SWBNNT obtained via optical spectra

analysis are well correlated with the obtained experimental data as presented in Table 4.

As shown in Table 4, all the literature showed that SWBNNT adsorbs hydrogen in the 5–15 eV range, which agrees well with our findings. SWCNT was also shown to adsorb in the 0 eV–5 eV range, which is also consistent with the current work. However, this work differs significantly from the previous reports as it took care of the geometry of the systems studied such as chirality, distance of the hydrogen molecule from the nanotubes and the diameter of the nanotubes.
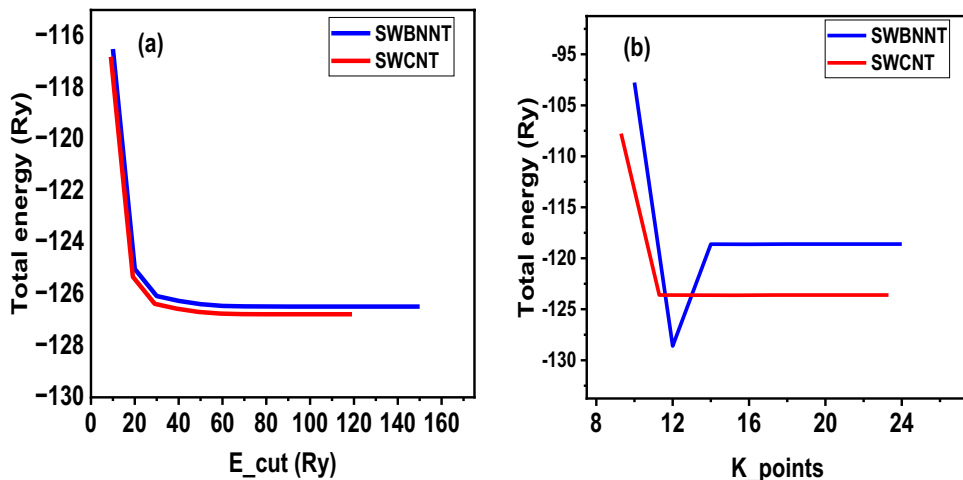
4 GW convergence

The self-energy of the SWCNT and SWBNNT electronic systems was determined using GW approximation in terms of one-particle green function G and screened Coulomb interaction W. Regarding kinetic energy cutoff

Table 4 Calculated and experimental data for hydrogen-adsorbed SWCNT and SWBNNT

Material	Method	Results and hydrogen storage energy range (eV)	Reference
SWCNT	Experimental Quartz crystal microbalance (QCM)	Adsorb more H_2 molecules than unpurified carbon nanotubes with a perfect hexagonal lattice in the range of 3–6 eV	[25]
	Spillover on graphene with Boron substitution	B-doping substantially enhanced H_2 adsorption in the visible region	[26]
	Optical spectra analysis	SWCNT adsorbs H_2 in all directions at the range of 0–5 eV. Revealed that adsorptions are due to the resettlement of H_2 molecules around the Fermi level. Also, microporous carbon has an enhanced hydrogen uptake via optical adsorption	Current work
SWBNNT	Ab initio theoretical	Adsorb in the range of 6–15 eV. Also, BNNT adsorbs H_2 due to the heteropolar binding nature of their atoms	[27]
	Experimental	Revealed hydrogen uptake capacities of 1.8 and 2.6 wt % and at 12 eV	[28]
	Optical spectra analysis	Revealed that SWBNNT adsorbs H_2 in an anisotropic manner at an energy range of 5–15 eV. Also, the adsorption of H_2 is due to the heteropolar binding nature of their atoms	Current work

Fig. 10 Convergence with respect to **a** kinetic energy cutoff and **b** k_Sampling grids

convergence as presented in Fig. 10a, one has to increase ecut values to at least 60 Ry to achieve convergence for both SWBNNT and SWCNT. Similarly, the convergence with respect to k_mesh for SwBNNT and SWCNT is presented in Fig. 10b. For good convergence, the k_grides must be at least 1 X 1 X 20. With respect to this work, we have set E_cut value of 125 Ry and k_point mesh of 1 X 1X 20 as the converged value for our calculations [29–33].

5 Conclusion

This work investigated the hydrogen adsorption properties of (8, 8) SWCNT and SWBNNT using popular density functional theory. The adsorption areas of the hydrogen molecule were chosen so that the hydrogen molecule was 8.72 away from each nanotube. From the present work, it was observed that well-converged values of hydrogen adsorption energies of − 537.06 eV and − 631.93 eV were achieved for (8, 8) SWCNT and SWBNNTs, respectively. Based on this, it can be reported that (8, 8) SWCNT provided a better adsorption surface area than (8, 8) SWBNNT. Analysis of optical adsorption spectra revealed that (8, 8) SWBNNT adsorbs hydrogen from visible to radio wave regions. The results of the optical interactions of (8, 8) SWCNT showed that the system absorbs hydrogen only in the visible region and exhibited optical adsorption properties similar to those of photocatalysts. Both (8, 8) SWCNT and SWBNNT gave off heat when adsorbing hydrogen due to direct transitions, while (8, 8) SWCNT generated light due to direct transitions. The results of this work indicated that while (8, 8) SWBNNT adsorbs more hydrogen than (8, 8) SWCNT, (8,8) SWCNT may be a better surface to store hydrogen in due to its ability to adsorb more in visible range and gives off no heat.

Data availability All data used in this work were contained in the manuscript.

Declarations

Conflict of interest The authors declare that they have no known competing financial interests or personal relationships that could have appeared to influence the work reported in this paper.

References

1. Frederica, P.: Pollution from fossil-fuel combustion is the leading environmental threat to global pediatric health and equity: solutions exist. Int. J. Environ. Res. Public. Health **15**, 16 (2018)
2. Caren, G., Renee, N., Debra, M., Chana, A., Thomas, H.: Fossil-fuel pollution and climate change—a new nejm group series. N. Engl. J. Med. **386**, 2328–2329 (2022)
3. Frederica, P., Kari, N.: Climate change, fossil-fuel pollution, and children's health. N. Engl. J. Med. **386**, 2303–2314 (2022)
4. Orazi, V., Ambrusi, R.E., Marchetti, J.M., Pronsato, M.E.: DFT study of the hydrogen adsorption and storage on Ni4 cluster embedded in multivacancy graphene. Int. J. Hydrog. Energy **45**(55), 30805–30817 (2020)
5. Yang, S., Wang, X., Lei, G., Xi, H., Zhao, W.: A DFT study on the outstanding hydrogen storage performance of the Ti-decorated MoS2 monolayer. Surf. Interfac. **26**, 101329 (2021)
6. Shivaprasad, K.V., Raviteja, S., Parashuram, C., Kumar, G.N.: Experimental Investigation of the Effect of Hydrogen Addition on Combustion Performance and Emissions Characteristics of a Spark Ignition High Speed Gasoline Engine. Procedia Technol. **14**, 141–148 (2014)
7. Pingping, L., Fangming, L., Yuan, P., Qiming, W.: A DFT study of hydrogen adsorption on Ca decorated hexagonal B36 with van der Waals corrections. Phys. E **114**, 113576 (2019)
8. Iqbal, S., Halima, K., Ashiq, H.P., Ahmad, S.: Recent development of carbon based materials for energy storage devices. Mater. Sci. Energy. Technol. **2**, 417–428 (2019)
9. Itas, Y.S., Suleiman, A.B., Razif, R., Aminu, S.Y.: Ab'initio studies of the structural and electronic properties for single-walled armchair MgONT, SiCNTs and ZnONTs for next generations' optoelectronics. Gadau J. Pure Allied Sci. **1**, 160–165 (2022)
10. Dario, et al.: Turbo charging time-dependent density-functional theory with Lanczos chains. J. Cheml Phys **128**, 154105 (2008)
11. Lawal, A., Shaari, A., Ahmad, R.: First-principles investigations of electron-hole inclusion effects on optoelectronic properties of Bi2Te3, a topological insulator for broadband photodetector. Physica B **520**, 69–75 (2017)
12. Ferdaus, A.J., Mayeen, K.U., Itas, Y.S., Miraz, M.H.: Cancerous and non-cancerous brain MRI classification method based on convolutional neural network and log-polar transformation. Healthcare **10**(9), 1801 (2022)
13. Blase, X., Rubio, A., Cohen, M.L.: Stability and band gap constancy of boron nitride nanotubes. EPL **28**, 335 (2014)
14. Itas, Y.S., Balarabe, A.S., Chifu, E.N., Lawal, A., Mayeen, K.U.: Computational studies of the excitonic and optical properties of armchair SWCNT and SWBNNT for optoelectronics applications. Crystals **12**(6), 870 (2022)
15. Itas, Y.S., Suleiman, A.B., Ebene, C.N., Lawal, A., Razif, R.: The exchange-correlation effects on the electronic bands of

hybrid armchair single-walled carbon boron nitride nanostructure. Crystals **12**(3), 394–394 (2022)

16. Arenal, R., Stephan, O., Kociak, M., Colliex, C.: Optical gap measurements of boron nitride nanotubes by EELS. Microsc. Microanal. **12**, 1166–1167 (2006)

17. Lönnecke, K., Eberhardt, O., Wallmersperger, T.: Electrostatic charge distribution in armchair and zigzag carbon nanotubes: a numerical comparison of CNT charge models. Acta Mech **21**, 03085–03093 (2021)

18. Jarvis, S.P., Taylor, S., Baran, J.D., Thompson, D., Saywell, A., Mangham, B., Champness, N.R., Larsson, J.A., Moriarty, P.: Physisorption controls the conformation and density of states of an adsorbed porphyrin. J. Phys. Chem. C **119**, 27982–27994 (2015)

19. Yahaya, S.I., Tasiu, Z., Ebene, C.N.: carbon nanotubes: a review of synthesis and characterization methods techniques. The Int J of Sci and Teck **8**(2), 111 (2020)

20. Jakub, K., Kupka, T., Marzena, J.: DFT studies on armchair (5, 5) SWCNT functionalization. modification of selected structural and spectroscopic parameters upon two-atom molecule attachment. J. Mol. Graph. Model. **55**, 105–114 (2015)

21. Itas, Y.S., Balarabe, A.S., Ebene, C.N., Lawal, A., Razif, R., Mayeen, K.U.: Effects of oxygen absorption on the electronic and optical properties of armchair and zigzag Silicon Carbide Nanotubes (SiCNTs). Phys. Scr. **98**, 015824 (2022)

22. Itas, Y.S., Ebene, C.N., Mayeen, K.U.: Synthesis of thermally stable h-bn-cnt hetero-structures via microwave heating of ethylene under nickel, iron, and silver catalysts. Crystal **11**(9), 1097 (2021)

23. Itas, Y.S., Isah, K.A., Nuhu, A.H., Razali, R., Salisu Tata, K.A., Naseer, A.M., Habib, I.M., Ullah and Mayeen Uddin Khandaker,: The potentials of boron-doped (nitrogen deficient) and nitrogen-doped (boron deficient) BNNT photocatalysts for decontamination of pollutants from water bodies. RSC Adv. **13**, 23659–23668 (2023)

24. Itas, Y.S., Razali, R., Tata, S., Idris, A.M., Khandaker, M.U.: Studies of the hydrogen energy storage potentials of Fe-and Al-doped silicon carbide nanotubes (SiCNTs) by optical adsorption spectra analysis. J. Energy Storage **71**, 108534 (2023)

25. Megan, C.: Eco-friendly hydrogen storage alternative with carbon nanotubes, Nanomaterials, (2022)

26. Hong, W., Fan, X., Kuo, J., Deng, W.: DFT Study of Hydrogen Storage by Spillover on Graphene with Boron Substitution. J. Phys. Chem. C **115**(18), 9241–9249 (2011)

27. Giannis, M., George, E.F.: Why boron nitride nanotubes are preferable to carbon nanotubes for hydrogen storage?: an ab initio theoretical study. Catal. Today **120**(3), 341–345 (2007)

28. Renzhi, M., Yoshio, B., Zhu, H., Xu, C.: Hydrogen uptake in boron nitride nanotubes at room temperature. J. Am. Chem. Soc. **124**(26), 7672–7673 (2002)

29. George, M., George, E.F.: DFT study of hydrogen storage by spillover with oxygen surface groups. J. Am. Chem. Soc. **131**(42), 15133–15135 (2009)

30. Fernando, H., Carlos, R.M., Jose, L.H.: Critical analysis on hydrogen as an alternative to fossil fuels and biofuels for vehicles in Europe. Renew. Sustain. Energy Rev. **14**, 772–780 (2010)

31. George, E.F.: Hydrogen storage in nanotubes & nanostructures. Mater. Today **14**, 324–328 (2011)

32. Itas, Y.S., Balarabe, A.S., Chifu, E.N., Lawal, A., Mayeen, K.U., Razif, R.: DFT studies of structural, electronic and optical properties of (5, 5) armchair magnesium oxide nanotubes (MgONTs). Phys E: Low-dimensional Syst Nanostruct. **149**, 115657 (2022)

33. Michael, R.M.: Titanium-decorated boron nitride nanotubes for hydrogen storage: a multiscale theoretical investigation. Nanoscale **11**, 16052–16062 (2019)